ORIGINAL ARTICLE

Using hyperpolarized ^{129}Xe MRI to quantify regional gas transfer in idiopathic pulmonary fibrosis

Jennifer M Wang,[1] Scott H Robertson,[2,3] Ziyi Wang,[2,4] Mu He,[2,5] Rohan S Virgincar,[2,4] Geoffry M Schrank,[2] Rose Marie Smigla,[6] Thomas G O'Riordan,[7] John Sundy,[7] Lukas Ebner,[8,9] Craig R Rackley,[6] Page McAdams,[9] Bastiaan Driehuys[2,3,4,9]

[1]School of Medicine, Duke University, Durham, North Carolina, USA
[2]Center for In Vivo Microscopy, Duke University Medical Center, Durham, North Carolina, USA
[3]Medical Physics Graduate Program, Duke University, Durham, North Carolina, USA
[4]Department of Biomedical Engineering, Duke University, Durham, North Carolina, USA
[5]Department of Electrical and Computer Engineering, Duke University, Durham, North Carolina, USA
[6]Department of Medicine, Division of Pulmonary, Allergy and Critical Care, Duke University Medical Center, Durham, North Carolina, USA
[7]Department of Respiratory Medicine, Gilead Sciences Inc, Foster City, California, USA
[8]Department of Radiology, University Hospital Inselspital, University of Bern, Bern, Switzerland
[9]Department of Radiology, Duke University Medical Center, Durham, North Carolina, USA

Correspondence to
Bastiaan Driehuys, Department of Radiology, Duke University Medical Center, Center for In Vivo Microscopy Box 3302, Durham, NC 27710, USA; bastiaan.driehuys@duke.edu

Received 27 January 2017
Revised 19 July 2017
Accepted 2 August 2017
Published Online First 31 August 2017

Linked

► http://dx.doi.org/10.1136/thoraxjnl-2017-210861

CrossMark

To cite: Wang JM, Robertson SH, Wang Z, *et al*. *Thorax* 2018;**73**:21–28.

ABSTRACT

Background Assessing functional impairment, therapeutic response and disease progression in patients with idiopathic pulmonary fibrosis (IPF) continues to be challenging. Hyperpolarized ^{129}Xe MRI can address this gap through its unique capability to image gas transfer three-dimensionally from airspaces to interstitial barrier tissues to red blood cells (RBCs). This must be validated by testing the degree to which it correlates with pulmonary function tests (PFTs) and CT scores, and its spatial distribution reflects known physiology and patterns of disease.

Methods 13 healthy individuals (33.6±15.7 years) and 12 patients with IPF (66.0±6.4 years) underwent ^{129}Xe MRI to generate three-dimensional quantitative maps depicting the ^{129}Xe ventilation distribution, its uptake in interstitial barrier tissues and its transfer to RBCs. For each map, mean values were correlated with PFTs and CT fibrosis scores, and their patterns were tested for the ability to depict functional gravitational gradients in healthy lung and to detect the known basal and peripheral predominance of disease in IPF.

Results ^{129}Xe MRI depicted functional impairment in patients with IPF, whose mean barrier uptake increased by 188% compared with the healthy reference population. ^{129}Xe MRI metrics correlated poorly and insignificantly with CT fibrosis scores but strongly with PFTs. Barrier uptake and RBC transfer both correlated significantly with diffusing capacity of the lungs for carbon monoxide ($r=-0.75$, $p<0.01$ and $r=0.72$, $p<0.01$), while their ratio (RBC/barrier) correlated most strongly ($r=0.94$, $p<0.01$). RBC transfer exhibited significant anterior-posterior gravitational gradients in healthy volunteers, but not in IPF, where it was significantly impaired in the basal ($p=0.02$) and subpleural ($p<0.01$) lung.

Conclusions Hyperpolarized ^{129}Xe MRI is a rapid and well-tolerated exam that provides region-specific quantification of interstitial barrier thickness and RBC transfer efficiency. With further development, it could become a robust tool for measuring disease progression and therapeutic response in patients with IPF, sensitively and non-invasively.

Key messages

What is the key question?
- How can we directly and sensitively measure the regional functional impairment caused by idiopathic pulmonary fibrosis (IPF)?

What is the bottom line?
- Hyperpolarised ^{129}Xe MRI provides non-invasive measures of pulmonary gas transfer at the alveolar capillary level that correlate robustly with diffusing capacity of the lungs for carbon monoxide, while revealing spatially resolved patterns of function that reflect a loss of gas transfer efficiency in the subpleural and basal lung in patients with IPF.

Why read on?
- ^{129}Xe MRI demonstrated three different patterns of impaired gas exchange that could represent different disease stages or phenotypes, which may aid in understanding the significant heterogeneity in disease courses often seen in IPF.

INTRODUCTION

Idiopathic pulmonary fibrosis (IPF), the most common interstitial pneumonia, is a devastating disease with a poor prognosis and estimated survival of 2–3 years after diagnosis.[1–3] Historically, treatment has been limited to lung transplantation,[1 4] but today, patients are routinely treated with anti-fibrotic therapy using either the tyrosine kinase inhibitor, nintedanib, or the tumour growth factor-beta inhibitor, pirfenidone.[1 5 6]

However, treatment of IPF and development of new therapies continue to be hampered by the lack of reliable metrics to assess therapeutic response and disease progression. To date, the primary indicators have been forced vital capacity (FVC) and diffusing capacity of the lungs for carbon monoxide (DL_{CO}).[1] While DL_{CO} measures gas exchange, it has been difficult to standardise in multi-institutional trials.[7] Thus, FVC is used as a surrogate endpoint in most clinical trials, despite the continued lack of consensus on a threshold to define clinically significant decline, predict outcomes and validate treatment decisions.[1 8–10]

The pathogenesis of IPF is thought to involve excess collagen deposition that limits the capacity of alveoli to participate in gas exchange.[4] However, the disease is heterogeneous in its distribution, and this cannot be captured using global metrics. Thus, imaging is needed to highlight and quantify disease activity regionally. To this end, high-resolution CT has become a mainstay in IPF, detecting fibrotic

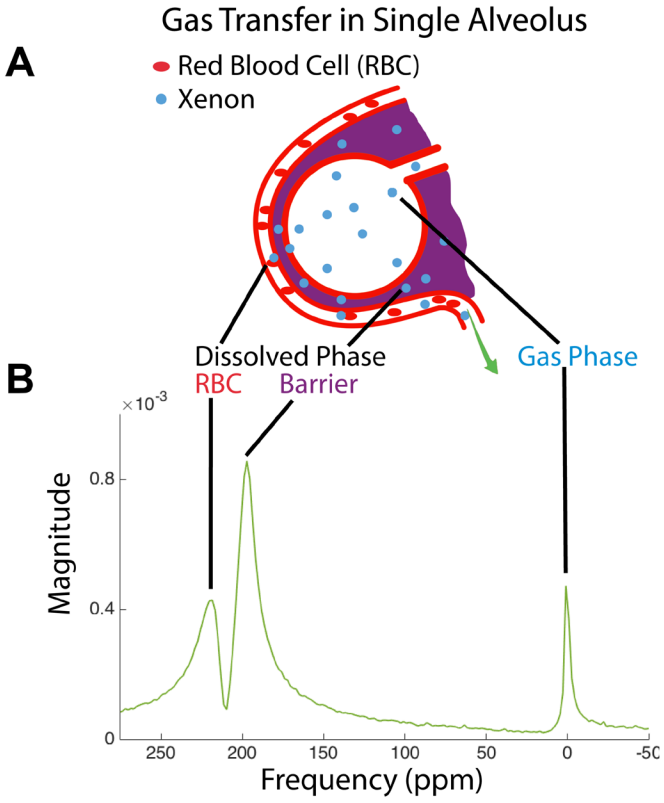

Figure 1 (A) Diagram of gas-phase ^{129}Xe transfer from alveoli to interstitial barrier tissues and capillary RBCs that comprise the dissolved phased signal. (B) The ^{129}Xe spectrum exhibits three resonances in lung at 0 ppm, 198 ppm and 217 ppm corresponding to ^{129}Xe in airspaces, dissolved in barrier and RBCs.

changes and structural abnormalities to establish the presence of a usual interstitial pneumonia (UIP) pattern without the need for surgical lung biopsies.[1] This has led to further interest in using quantitative CT to measure longitudinal change, assess disease severity and predict mortality.[11–13] However, the structural alterations detected on CT often do not correlate well with patient symptoms.[14]

A promising modality by which to assess regional function is MRI using inhaled hyperpolarized (HP) ^{129}Xe gas. This method is rapid, well tolerated[15] and allows for gas uptake and transfer to be assessed in a spatially resolved manner. On inhalation, xenon diffuses from the alveoli, through pulmonary barrier tissues comprised of alveolar epithelial cells, interstitial tissues, capillary endothelial cells, and plasma, and finally into capillary red blood cells (RBCs). Moreover, in each of these compartments, ^{129}Xe exhibits distinct resonance frequency shifts[16 17] (figure 1A,B) that enable its uptake in them to be measured separately.[18–22]

Previously, whole-lung spectroscopic measurements demonstrated that the ratio of ^{129}Xe uptake in RBCs versus barrier was dramatically reduced in subjects with IPF compared with healthy volunteers.[17] This work was subsequently extended to produce isotropic three-dimensional (3D) images of ^{129}Xe in the airspaces, barrier and RBCs and qualitatively revealed that RBC signal was diminished or absent in regions where fibrosis was evident on CT.[23] We have since developed methods that quantify ^{129}Xe transfer MRI more rigorously to reveal preliminary evidence that in IPF ^{129}Xe uptake in the barrier tissues is also significantly enhanced.[24]

In this work we sought to determine the correlation between biomarkers derived from quantitative ^{129}Xe gas transfer MRI and established metrics and to characterise the spatial distribution of ^{129}Xe gas transfer impairment. We hypothesised that ^{129}Xe biomarkers would correlate more strongly with the pulmonary function test (PFT) measurements, FVC and DL_{CO}, than with CT fibrosis scores.[25] Furthermore, we hypothesised that the spatial distribution of ^{129}Xe gas transfer MRI would follow known histopathological patterns in IPF. Specifically, we tested the hypothesis that enhancement of barrier uptake and impairment of RBC transfer would predominate in the basal and subpleural lung.[1 26 27]

METHODS

Subject recruitment

This study was approved by the Duke Institutional Review Board. Written, informed consent was obtained from each subject prior to protocol recruitment. Data were acquired from 13 healthy volunteers (33.6±15.7 years, 9 men, 4 women) and 12 subjects with IPF (66.0±6.4 years, 10 men, 2 women). All subjects were at least 18 years old and had no history of cardiac arrhythmias. Healthy volunteers had no smoking history or diagnosed pulmonary conditions. All subjects underwent baseline pulmonary function testing to obtain FVC by spirometry and DL_{CO} by the single-breath method. The diagnosis of IPF was determined using ATS criteria confirming a UIP pattern on CT or from surgical lung biopsy.[1] All subjects with IPF had prior CT scans, with an interval of 5.1±4.9 months from their MRI scan. CT scans were evaluated by a chest radiologist using established criteria to produce a mean fibrosis score ranging from 0% to 100%.[25] These scores were used to classify IPF disease severity as mild (<11%), moderate (11%–30%) or severe (>30%).[25]

^{129}Xe polarisation and delivery

Isotopically enriched ^{129}Xe gas (85%) was polarised to 20% (Model 2881, Polarean, Durham, North Carolina, USA) and dispensed into a Tedlar dose delivery bag as previously described.[28] Subjects received a small dose (51 mL dose equivalent of pure HP ^{129}Xe) for calibration and a larger dose (85 mL dose equivalent) for the imaging scan.[29] These doses required xenon volumes ranging from 300 to 750 mL, which were expanded with high-purity helium to achieve a net 1 L volume, which subjects inhaled from functional residual capacity. They then held their breath for 13–15 s during scanning, while heart rate and oxygen saturation were monitored with an MR-compatible monitoring system (Expression Model 865214, Invivo, Orlando, Florida, USA).

Image acquisition and reconstruction

^{129}Xe gas transfer MRI was acquired on a 1.5T scanner (GE EXCITE 15M4), using an interleaved radial acquisition of gas-phase and dissolved-phase images during a 15 s breath-hold.[30] Images were acquired at an echo time (TE_{90}≈ 0.9 ms) that allows the barrier and RBC signals to be separated by the 1-point Dixon method.[23] This generated separate isotropic 3D images of the gas, barrier and RBC compartments with 6.3 mm isotropic voxels.

Image processing and analysis

The gas-phase images were rendered into quantitative maps by rescaling by their top percentile of intensities and assigning each voxel into one of six colour clusters. These clusters each span an intensity range equal to one SD of the ventilation reference distribution derived from a healthy cohort.[31] The barrier and RBC images were divided on a voxel-by-voxel basis by the gas-phase intensities to create maps of barrier uptake and RBC transfer. These

maps were also cast into colour clusters, each spanning one SD of the associated healthy cohort reference distribution as recently detailed.[24] The resulting barrier maps reflect the amount of ^{129}Xe uptake in interstitial tissues compared with healthy subjects. Similarly, the RBC transfer maps depict the amount of ^{129}Xe that has reached the capillary RBCs, again relative to a healthy cohort. Each map was quantified by its mean, as well as by the percentage of voxels in the highest and lowest two clusters of their distribution. For barrier maps, the highest two clusters ($Barrier_{High}$) contained the percentage of voxels falling three or more SD above the healthy reference mean. This metric thus reflected interstitial thickening. For the RBC maps, the lowest two clusters (RBC_{Low}) contained the percentage of voxels falling more than one SD below the reference mean. This metric thus quantified the fraction of lung exhibiting poor gas transfer to RBCs.

Functional gradient analysis

To test the validity of the spatial distribution in functional gas transfer MRI, signal gradients were quantified in three directions. First, the lungs were divided into two equal volumes in the anterior/posterior direction to test the hypothesis that gravitational effects that increase tissue density and perfusion to the dependent lung in healthy subjects would be eliminated in IPF. Similarly, gradients were calculated in the apical/basal direction to assess the hypothesis that impaired function in IPF would show a basal predominance,[26] and finally gradients in the central/peripheral direction were calculated to test the hypothesis that impaired function would also follow a peripheral predominance.[27] This was done by defining the peripheral lung as the outermost 2–3 cm of the subpleural lung perimeter. All spatial gradients were calculated by dividing the mean signal difference between regions by their average.

Statistical methods

All statistical analyses were performed using JMP 12 (SAS Institute, Cary, North Carolina, USA). The unpaired two-tailed Student's t-test was used to evaluate differences in the spatial distribution of gas transfer. Linear regression analysis and the Pearson correlation coefficient (r) were used to assess correlation between functional MRI metrics and CT fibrosis scores, as well as PFT results. For all comparisons, the level of significance was 5% ($p<0.05$).

RESULTS

Single-breath, isotropic images of gas and dissolved-phase ^{129}Xe were successfully acquired in all subjects and reliably decomposed into separate ventilation, barrier uptake and RBC transfer maps. Subject demographics, PFT results and functional imaging-derived ratios are summarised in table 1.

Representative gas transfer maps in healthy subjects versus subjects with IPF

Representative ventilation, gas transfer maps and CT images are depicted in figure 2A for a healthy control subject (FVC=97% predicted, DL_{CO}=113% predicted). All maps consist largely of green voxels that represent ratios falling within ±1 standard deviation of the reference healthy mean. While all maps exhibited mean values close to the reference mean (ventilation=93%, barrier=120%, RBC=121%), they do exhibit notable gradients as both barrier uptake and RBC transfer increase towards the gravitationally dependent lung. However, only a modest percentage of voxels fell into $Barrier_{High}$ (0.5%) and RBC_{Low} (10%). Low RBC transfer was seen primarily in the anterior, non-gravitationally dependent lung. This pattern of few pixels falling in $Barrier_{High}$ and RBC_{Low} was generally found to exist in the healthy cohort as shown in table 1.

Table 1 Subject demographics, PFT metrics and imaging-derived parameters

	Healthy	IPF
Subject demographics		
Number	13	12
Male/female	9/4	10/2
Age	33.6±15.7	66.0±6.4
Pulmonary function tests		
FVC (L)	4.1±0.9	2.6±0.8
FVC % predicted	94±15	65±19
DL_{CO} (mL/min/mm Hg)	26±6.0	11±3.2
DL_{CO} % predicted	93±17	48±14
Xenon transfer metrics		
$Ventilation_{Mean}$	0.51±0.06	0.45±0.06
% $Reference_{Mean}$	99±11	88±11
$Barrier_{Mean}$ ($\times10^{-2}$)	0.52±0.13	0.91±0.17
% $Reference_{Mean}$	106±26	188±36
$Barrier_{High}$ %	3.0±8.0	48.7±32.2
RBC_{Mean} ($\times10^{-2}$)	0.28±0.06	0.19±0.06
% $Reference_{Mean}$	108±23	72±25
RBC_{Low} %	14.6±6.9	41.9±21.2
$RBC/barrier_{Mean}$	0.58±0.13	0.21±0.07
% $Reference_{Mean}$	108±24	40±12
CT metrics		
CT fibrosis score %	N/A	17.4±12.2

Values listed are in the format mean±SD. The %$Reference_{Mean}$ values are compared relative to reference values derived from a cohort of healthy volunteers.
DL_{CO}, diffusing capacity of the lungs for carbon monoxide; FVC, forced vital capacity; IPF, idiopathic pulmonary fibrosis; RBC, red blood cell.

Figure 2B depicts ^{129}Xe functional maps in a subject with moderate IPF (FVC=55% predicted, DL_{CO}=31% predicted, CT fibrosis score=25.4%). Although ventilation (mean=91%) was not significantly different from the healthy volunteer, the barrier signal was strikingly enhanced throughout the lung (206% of reference), with 74% of voxels falling in $Barrier_{High}$. Enhanced barrier uptake was most notable in the subpleural regions, which was accompanied by reduced RBC transfer (57% of reference), with 52% falling into RBC_{Low}. The corresponding CT images depict predominantly basal and peripheral reticulation and areas of ground glass attenuation, with mild traction bronchiectasis in the affected areas.

Figure 2C depicts ventilation and gas transfer maps in a patient with severe IPF (FVC=42% predicted, DL_{CO}=23% predicted, CT fibrosis score=34.2%). Ventilation maps have a reduced mean (83% of reference), but the most striking feature is the highly elevated barrier uptake throughout most of the lung (200% of reference, $Barrier_{High}$=65%). Similarly, this subject exhibited significant regions of low RBC transfer (49% of reference and RBC_{Low}=65%). Low RBC transfer was most evident in the posterior and basilar lung. These matched well with extensive distortion of the lung architecture and honeycombing seen on CT. Interestingly, in portions of these posterior slices, the barrier uptake was in the normal range.

Figure 2D shows ventilation and gas transfer maps in another IPF subject with severe disease (FVC=62% predicted,

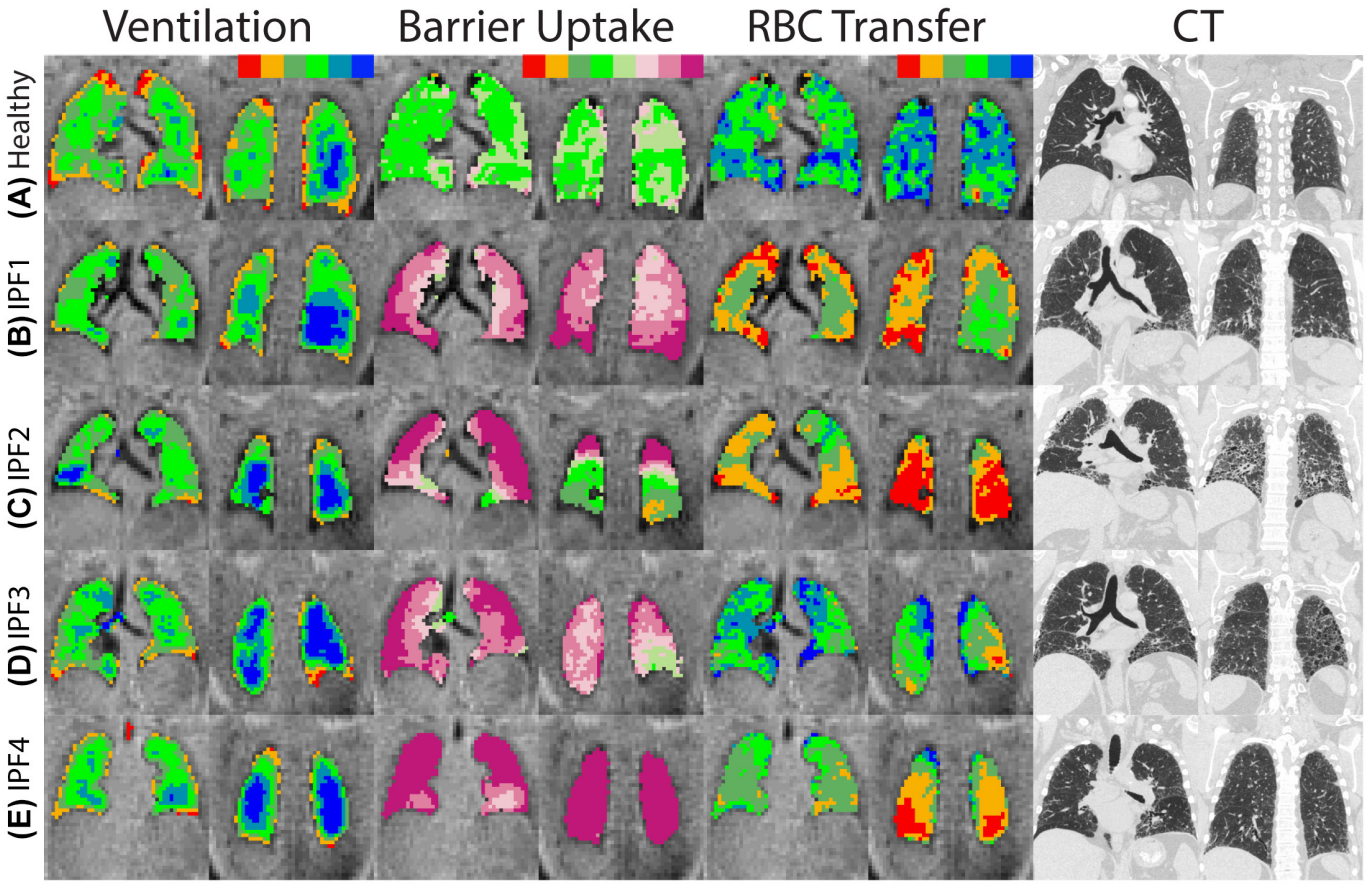

Figure 2 Central and posterior coronal slices of ventilation (red=ventilation defects, blue=high), barrier uptake (red=low, plum/orchid=high) and RBC transfer (red=low, blue=high), binning maps and CT images in one healthy subject and four subjects with IPF. (A) Healthy subject with FVC=97%, DL_{CO}=113%, $Barrier_{High}$=0.5%, RBC_{Low}=10%. (B) IPF subject 1 with FVC=55%, DL_{CO}=31%, $Barrier_{High}$=74%, RBC_{Low}=52%, CT fibrosis score=25.4%. (C) IPF subject 2 with FVC=42%, DL_{CO}=23%, $Barrier_{High}$=65%, RBC_{Low}=65%, CT fibrosis score=34.2%. (D) IPF subject 3 with FVC=62%, DL_{CO}=47%, $Barrier_{High}$=61%, RBC_{Low}=18%, CT fibrosis score=46.7%. (E) IPF subject 4 with FVC=77%, DL_{CO}=54%, $Barrier_{High}$=94%, RBC_{Low}=36%, CT fibrosis score=10.4%. DL_{CO}, diffusing capacity of the lungs for carbon monoxide; FVC, forced vital capacity; IPF, idiopathic pulmonary fibrosis; RBC, red blood cell.

DL_{CO}=47% predicted, CT fibrosis score=46.7%). Here, ventilation is preserved (104% of reference), but barrier maps again exhibit significant enhancement throughout the lung (196% of reference, $Barrier_{High}$=61%). However, ^{129}Xe transfer to RBCs remained in the normal range through most of the lung, with a mean that exceeded the reference value (114%). Only a few regions of low RBC transfer were evident in the peripheral and posterior lung (RBC_{Low}=18%). This patient had a CT scan notable for honeycombing and parenchymal changes consistent with a UIP pattern.

Figure 2E shows an IPF subject with mild disease (CT fibrosis score=10.4%) and the highest FVC (77% predicted) and DL_{CO} (54% predicted) in the cohort. Again, ventilation maps resemble those of healthy subjects (104% of reference). However, this subject also exhibited the highest barrier uptake in the cohort (246% of reference, $Barrier_{High}$=94%). The RBC maps depict normal gas transfer in the midlung but otherwise low RBC transfer in the apical and basal lung (mean=73%, RBC_{Low}=36%.) In this patient with biopsy-confirmed UIP, CT showed a possible UIP pattern with a peripheral reticular pattern and mild traction bronchiectasis but no honeycombing.

Correlation with CT fibrosis scores

In most subjects with IPF, the spatial correlation between functional ^{129}Xe transfer metrics and CT was not immediately evident. CT fibrosis score was weakly and insignificantly correlated with all MRI metrics: ventilation (r=0.09, p=0.77), barrier uptake (r=0.27, p=0.38), RBC transfer (r=0.21, p=0.48) and RBC/barrier ratio (r=−0.05, p=0.88).

Correlation with pulmonary function tests

Almost all image-derived average gas transfer metrics, ventilation, barrier uptake, RBC transfer and RBC/barrier ratio, correlated significantly with FVC and DL_{CO} (figure 3); the only exception was between ventilation and DL_{CO}. Ventilation correlated moderately and positively with FVC (r=0.39, p=0.04) but not significantly with DL_{CO} (r=0.35, p=0.06). Barrier uptake correlated negatively and significantly with both FVC (r=−0.61, p<0.01) and DL_{CO} (r=−0.75, p<0.01). RBC transfer correlated positively and significantly with both FVC (r=0.63, p<0.01) and DL_{CO} (r=0.72, p<0.01). Overall, the strongest correlation was between RBC/barrier ratio and DL_{CO} (r=0.94, p<0.01).

Spatial patterns of gas transfer

Although ^{129}Xe gas transfer metrics did not correlate with structural CT scores, spatial gradients in ^{129}Xe gas transfer followed expected patterns (figure 4). Ventilation maps in both cohorts demonstrated increasing intensity from the anterior to posterior and apical to basal directions but decreasing intensity from the central to peripheral direction. However, none of these gradients were significantly different between healthy subjects and subjects with IPF. Notably,

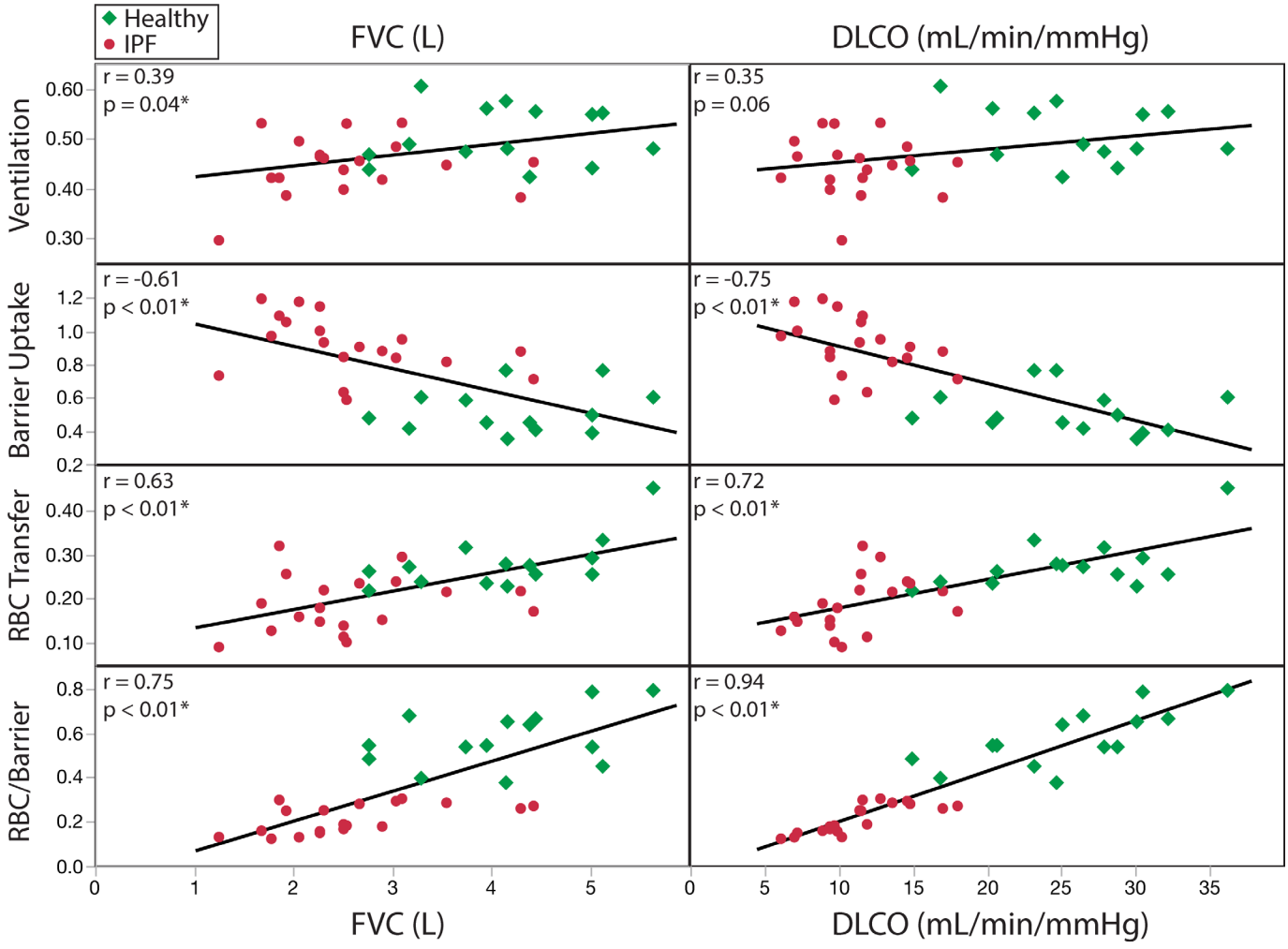

Figure 3 Mean ^{129}Xe ventilation correlates only modestly with FVC and DL_{CO}. However, barrier uptake, RBC transfer and RBC/barrier ratio all correlate well with FVC and DL_{CO}. The correlation between RBC/barrier and DL_{CO} (r=0.94) is particularly strong. In subjects with more than one MRI scan, correlation coefficients were calculated using all scans, while p values were derived using only the most recent time point to avoid assuming the independence of multiple measurements. DL_{CO}, diffusing capacity of the lungs for carbon monoxide; FVC, forced vital capacity; IPF, idiopathic pulmonary fibrosis; RBC, red blood cell.

barrier uptake exhibited a significantly stronger anterior to posterior gradient in healthy volunteers (22%) than subjects with IPF (8%, p<0.01). Yet, in the apical/basal or central/peripheral directions, barrier gradients were subtle (<10%) and were not significantly different between healthy subjects and subjects with IPF (p=0.63 and p=0.35, respectively). RBC transfer was characterised by a strong anterior to posterior gradient in healthy controls (mean=32%) that was eliminated in IPF (mean=2%, p<0.01). However, in IPF, RBC transfer exhibited a strong apical to basal gradient (−36%), significantly greater than in healthy volunteers (−12%, p=0.02). RBC transfer also exhibited a stronger central-peripheral gradient in IPF (−22%) than in healthy volunteers (−10%, p<0.01).

DISCUSSION

PFT correlations support functional imaging findings

The primary tools for diagnosing and monitoring IPF disease progression continue to be a combination of PFTs, CT scans and 6 min walk testing. Thus, the observation that ventilation MRI correlated only weakly with DL_{CO} and insignificantly with FVC suggests that its regional assessment does not provide a meaningful measure of disease severity in IPF. However, it is noteworthy that ^{129}Xe MRI-derived barrier uptake, RBC transfer and RBC/barrier ratio correlated well with DL_{CO}, a direct marker of global gas exchange. In particular, RBC/barrier was exceptionally well-correlated (r=0.94), thereby conferring it with a strong physiological grounding. Unlike DL_{CO}, however, RBC/barrier can be further dissected to identify changes in barrier and RBC transfer individually, as well as how these are distributed regionally. Moreover, because these metrics are calculated using signals localised within the airspaces, this inherently accounts for differences in the volume of inhaled xenon, making it potentially less effort dependent.[32]

Functional ^{129}Xe MRI complements structural CT findings

The poor correlation between ^{129}Xe MRI functional metrics and CT structural scores was particularly surprising. It is possible that these scores (which also correlated weakly and non-significantly with PFTs) reflect a limitation of the reader-based methodology. Recently, such reader methods were found inferior to computer-based CT analysis in predicting mortality in IPF,[33] and one larger-scale study reported such more sophisticated densitometric and feature-based analysis to correlate positively with PFTs.[34] However, a more fundamental explanation is that ^{129}Xe MRI signal in barrier and RBC inherently arises only from the

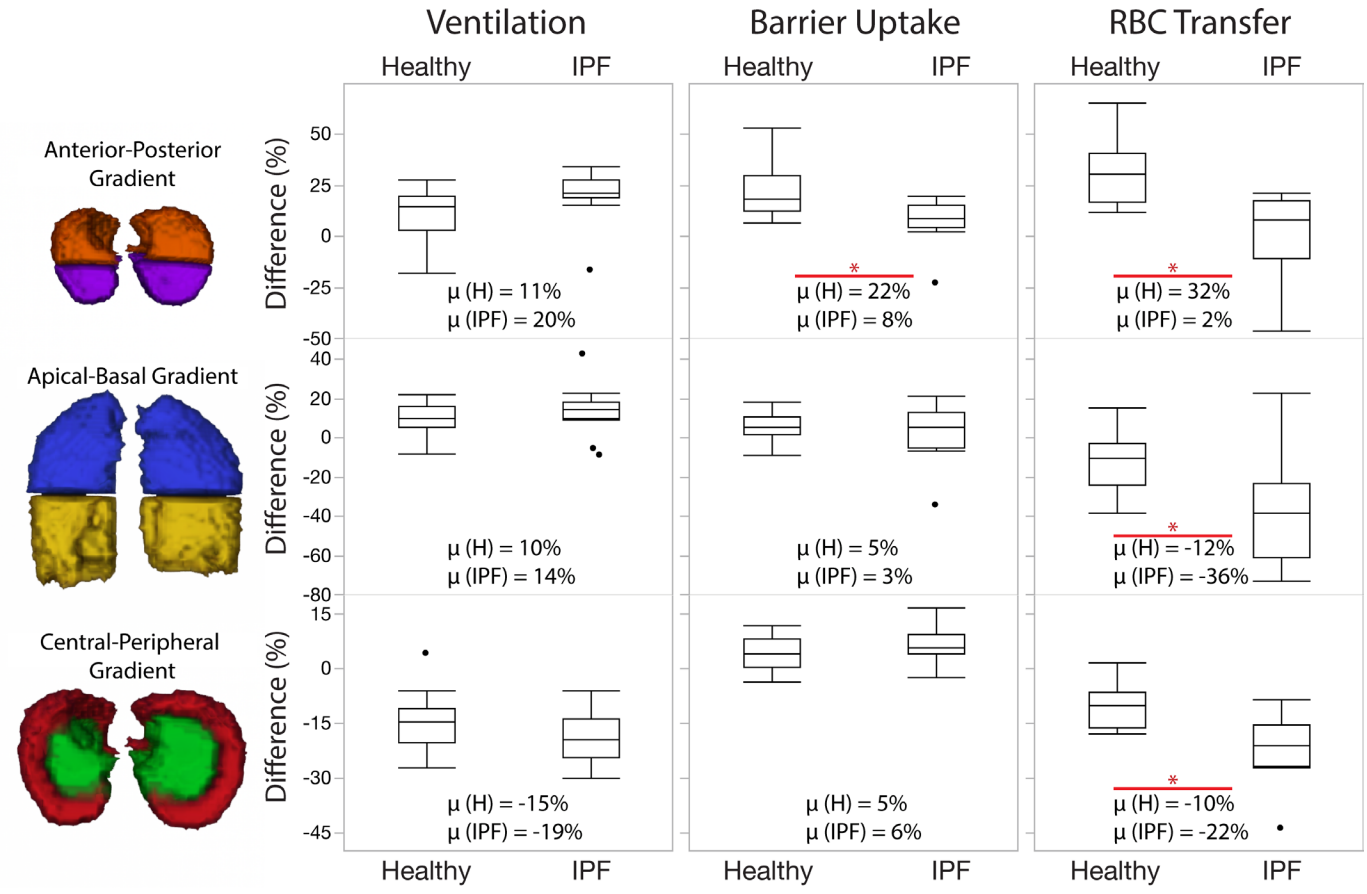

Figure 4 Ventilation, barrier uptake and RBC transfer gradients in three directions. In both healthy subjects and subjects with IPF, ventilation gradients follow similar spatial patterns. Barrier transfer exhibits a spatial gradient only in the anterior-posterior direction of gravity and only in healthy lungs. A similar but stronger gradient in RBC transfer was present in healthy subjects but absent in IPF. In IPF, RBC transfer follows a large apical/basal gradient and a moderate central/peripheral gradient, consistent with known patterns of disease. IPF, idiopathic pulmonary fibrosis; RBC, red blood cell. μ - average difference, H - healthy, *statistically significant.

alveolar capillary unit and thus directly probes its function.[35] Thus, one possible interpretation is that these direct regional gas exchange measurements are sensitive to disease at the alveolar level, which can differ from what might be inferred from large-scale structural findings on high-resolution CT.

The primary exception to the poor correlation between ^{129}Xe MRI and CT was in late-stage IPF, where they appeared to agree visually, particularly in regions exhibiting extensive honeycombing. In such regions, both barrier uptake and RBC transfer were often diminished or absent. However, in less severe IPF, agreement was considerably weaker. In our cohort, we found numerous patients with definite UIP patterns on CT that did not demonstrate significantly impaired RBC transfer. In such cases, MRI paints a picture of preserved lung function despite extensive structural injury. On the other end of the spectrum, we also observed subjects where structural abnormalities were relatively few, but where MRI exhibited massive barrier enhancement throughout the lung, paired with regionally impaired RBC transfer. This may indicate significant disease activity that has not yet irreversibly remodelled the lung architecture.

Functional imaging gradients consistent with normal physiology and fibrosis distribution

It is encouraging that ^{129}Xe MRI reveals spatial gradients that are consistent with both normal pulmonary physiology and the typical spatial patterns of disease in IPF. In a healthy subject lying supine, perfusion follows a gravitational gradient favouring the posterior lung.[36] This was reflected in healthy volunteers exhibiting generally robust RBC transfer in the dependent lung, while any regions of low transfer were generally confined to the non-dependent, anterior slices. Similarly, barrier uptake also favoured the dependent lung in healthy subjects.

By contrast, such physiological gradients in ^{129}Xe gas transfer were absent in IPF. Instead, barrier uptake was enhanced throughout the lung, consistent with a widespread pattern of fibrosis[4] serving to override gravitational effects. Similarly, RBC transfer did not exhibit a gravitationally dependent pattern in IPF, possibly reflecting recruitment of gas exchange to anterior lung regions to maintain stable lung function.[37] However, in the IPF cohort, several ^{129}Xe spatial gradients emerged that were different from the healthy population. In particular, RBC transfer was significantly diminished in the basal and peripheral lung. This is where fibrosis and honeycombing are most commonly found on histology and CT.[1 27]

Models of gas transfer in IPF

^{129}Xe MRI revealed four distinct patterns of gas exchange that often coexisted in the same patient (figure 5). The first is the essentially normal unit that predominates in healthy individuals (figure 5A), where inhaled ^{129}Xe freely diffuses from the alveoli through the thin alveolar–capillary barrier to reach circulating RBCs. This results in barrier and RBC transfer being in the

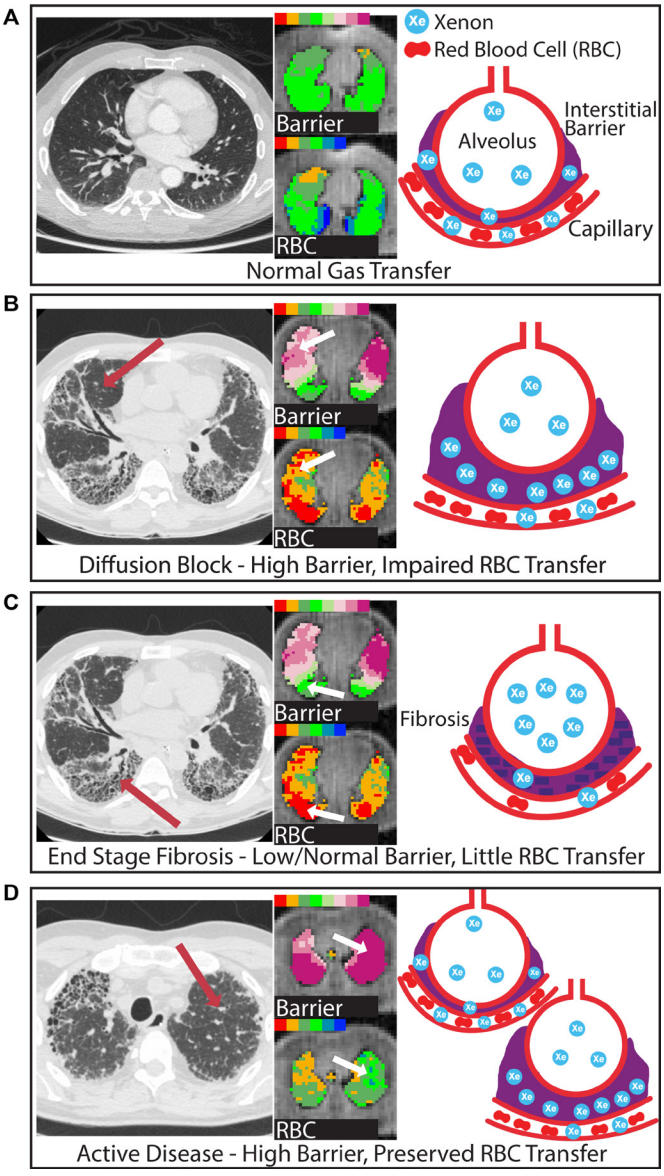

Figure 5 Proposed models of gas transfer for various barrier uptake (red=low, plum/orchid=high) and RBC transfer patterns (red=low, blue=high). In a healthy lung (A), gaseous ^{129}Xe efficiently diffuses from the alveolus, across a thin barrier to RBCs, resulting in signal intensities in the normal range for both compartments. In IPF, however, interstitial fibrosis thickens the barrier tissue, which increases xenon uptake. In some regions of barrier enhancement (B, arrows), diffusion across it is slowed, causing RBC transfer to decrease. As the disease progresses (C), scarring becomes so severe that ^{129}Xe no longer diffuses into or through the barrier. Therefore, barrier uptake returns to the normal or low range, while RBC transfer is dramatically reduced. Most interesting are regions depicting the coexistence of increased barrier uptake with preserved RBC transfer (D, arrow). This may represent regions of disease activity that could be responsive to therapy.

normal (green) range. Next is a region consistent with the classical model of diffusion limitation (figure 5B), where thickening of the alveolar–capillary membrane increases barrier uptake and delays transfer to capillary RBCs.[17] Note that while xenon is classically considered to be a perfusion-limited gas, HP ^{129}Xe MRI is inherently sensitive to diffusion impairment.[17]

Figure 5C depicts a pattern that is seen in subjects with end-stage disease, characterised by regions with seemingly normal or even low barrier uptake but almost no RBC transfer. When examined on CT, these regions reveal severe fibrosis and honeycombing. We suggest that such regions represent severe and permanent scarring that impairs ^{129}Xe uptake into the barrier tissue, thereby almost entirely eliminating its subsequent transfer to RBCs. Over time, such distortion would likely also lead to absent perfusion.

Moreover, perhaps most interesting, is figure 5D, which illustrates a pattern of greatly enhanced barrier uptake coexisting with preserved RBC transfer. This is unexpected from conventional models in which a thicker barrier should impair gas transfer to RBCs. However, this finding agrees with histological patterns of IPF, where patchy fibrotic zones, honeycomb changes and fibroblastic foci are known to coexist with regions of normal lung.[38 39] Given the relatively modest resolution of the images (250 mm^3), a single voxel contains over 40 000 alveoli, many of which could plausibly be normal.[40] Combined with the known histopathological temporal heterogeneity in IPF, this pattern may represent early disease where fibrotic changes are below the resolution of conventional CT. Such at-risk regions may be particularly valuable to monitor as IPF progresses and could help identify areas where novel therapies may elicit a positive response.

Study limitations and future directions

Although ^{129}Xe MRI shows promise in delivering a wealth of regional functional information, it will be critical to apply these methods to larger cohorts and to establish short-term reproducibility. In the present study, we can only estimate an initial upper bound on variability by examining one healthy subject and seven subjects with IPF in the study who were scanned at two time points (average 7.7 months apart). This yielded within-subject coefficients of variation of ±16% for barrier uptake, ±18% for RBC transfer and ±11% for RBC/barrier. However, given that this sample includes several patients with IPF who exhibited significant clinical disease progression between scans, this crude estimate clearly represents only an upper bound. Perhaps a more representative benchmark is the whole-lung RBC/barrier spectroscopic ratio, which was previously shown to exhibit a same day variability of ±6.6%.[17]

One limitation of our study was the use of younger subjects in our control group. Although this provides a useful starting reference, the ageing lung is known to undergo physiological changes in chest wall compliance, respiratory muscle function and the lung parenchyma, all with the potential to affect gas exchange.[41 42] Thus, future studies may benefit from including an older, age-matched population of healthy controls. Furthermore, all subjects inhaled 1 L of gas regardless of their lung volumes, which may affect our functional metrics. However, in our preliminary studies of healthy individuals scanned at both Functional Residual Capacity (FRC) + 1 L and after deliberate exhalation to FRC, gas transfer patterns were largely unchanged. Future studies would also benefit from determining and correcting for patient-specific haemoglobin levels.

We note several possible limitations that could explain the much stronger correlation of ^{129}Xe MRI to PFTs. First, CT scoring was only available in the IPF cohort. However, even when eliminating healthy subjects from analysis, the ^{129}Xe-PFT correlations remained robust for RBC/barrier with FVC ($r=0.57$, $p=0.01$) and DL_{CO} ($r=0.80$, $p=0.01$). We also note that several subjects in the IPF cohort had CT and MRI scans several months apart. However, other studies of quantitative CT biomarkers in IPF detected changes in CT score over a 7-month period of

2%–3%.[11] Thus, we expect the average 5-month separation of scans to be an unlikely explanation for the lack of correlation with ^{129}Xe MRI.

CONCLUSIONS

These preliminary data suggest that ^{129}Xe gas transfer MRI has the potential to add new insight by visualising functional change regionally. Because the method is non-invasive and avoids ionising radiation, it can be further developed to deliver robust and reproducible metrics to meet the pressing need for more sensitive markers of IPF disease activity. As a research tool, ^{129}Xe MRI provides a fundamentally new way to characterise disease pathophysiology, which could translate to become clinically valuable in our efforts to understand the effects of emerging therapies and the mechanisms behind lung injury in IPF.

Acknowledgements The authors wish to thank Sally Zimney for proofreading the manuscript.

Contributors CRR, PM and BD designed and implemented the study. JMW, SHR, ZW, MH, RSV, GMS and BD collected the data. JMW, SHR, ZW, MH and BD were responsible for data analysis. All authors contributed to the writing of the manuscript.

Funding Research reported in this publication was supported by the NIH/NHLBI R01HL105643 and R01HL126771, the Duke Center for In Vivo Microscopy, an NIH/NIBIB National Biomedical Technology Resource Center (P41 EB015897) and Gilead Sciences. LE received financial funding by the Swiss National Science Foundation.

Competing interests BD is founder and shareholder in Polarean Imaging, a company established to commercialise hyperpolarised ^{129}Xe MRI technology.

Ethics approval This study was approved by the Duke Institutional Review Board.

Provenance and peer review Not commissioned; externally peer reviewed.

REFERENCES

1 Raghu G, Collard HR, Egan JJ, *et al*. An official ATS/ERS/JRS/ALAT statement: idiopathic pulmonary fibrosis: evidence-based guidelines for diagnosis and management. *Am J Respir Crit Care Med* 2011;183:788–824.
2 Flaherty KR, Toews GB, Travis WD, *et al*. Clinical significance of histological classification of idiopathic interstitial pneumonia. *Eur Respir J* 2002;19:275–83.
3 Nicholson AG, Colby TV, du Bois RM, *et al*. The prognostic significance of the histologic pattern of interstitial pneumonia in patients presenting with the clinical entity of cryptogenic fibrosing alveolitis. *Am J Respir Crit Care Med* 2000;162:2213–7.
4 King TE, Pardo A, Selman M. Idiopathic pulmonary fibrosis. *Lancet* 2011;378:1949–61.
5 King TE, Bradford WZ, Castro-Bernardini S, *et al*. A phase 3 trial of pirfenidone in patients with idiopathic pulmonary fibrosis. *N Engl J Med* 2014;370:2083–92.
6 Richeldi L, du Bois RM, Raghu G, *et al*. Efficacy and safety of nintedanib in idiopathic pulmonary fibrosis. *N Engl J Med* 2014;370:2071–82.
7 Jensen RL, Teeter JG, England RD, *et al*. Instrument accuracy and reproducibility in measurements of pulmonary function. *Chest* 2007;132:388–95.
8 Richeldi L, Ryerson CJ, Lee JS, *et al*. Relative versus absolute change in forced vital capacity in idiopathic pulmonary fibrosis. *Thorax* 2012;67:407–11.
9 Zappala CJ, Latsi PI, Nicholson AG, *et al*. Marginal decline in forced vital capacity is associated with a poor outcome in idiopathic pulmonary fibrosis. *Eur Respir J* 2010;35:830–6.
10 du Bois RM, Weycker D, Albera C, *et al*. Forced vital capacity in patients with idiopathic pulmonary fibrosis: test properties and minimal clinically important difference. *Am J Respir Crit Care Med* 2011;184:1382–9.
11 Kim HJ, Brown MS, Chong D, *et al*. Comparison of the quantitative CT imaging biomarkers of idiopathic pulmonary fibrosis at baseline and early change with an interval of 7 months. *Acad Radiol* 2015;22:70–80.
12 Best AC, Meng J, Lynch AM, *et al*. Idiopathic pulmonary fibrosis: physiologic tests, quantitative CT indexes, and CT visual scores as predictors of mortality. *Radiology* 2008;246:935–40.
13 Maldonado F, Moua T, Rajagopalan S, *et al*. Automated quantification of radiological patterns predicts survival in idiopathic pulmonary fibrosis. *Eur Respir J* 2014;43:204–12.
14 Mura M, Ferretti A, Ferro O, *et al*. Functional predictors of exertional dyspnea, 6-min walking distance and HRCT fibrosis score in idiopathic pulmonary fibrosis. *Respiration* 2006;73:495–502.
15 Driehuys B, Martinez-Jimenez S, Cleveland ZI, *et al*. Chronic obstructive pulmonary disease: safety and tolerability of hyperpolarized 129Xe MR imaging in healthy volunteers and patients. *Radiology* 2012;262:279–89.
16 Chen RY, Fan FC, Kim S, *et al*. Tissue-blood partition coefficient for xenon: temperature and hematocrit dependence. *J Appl Physiol Respir Environ Exerc Physiol* 1980;49:178–83.
17 Kaushik SS, Freeman MS, Yoon SW, *et al*. Measuring diffusion limitation with a perfusion-limited gas--hyperpolarized 129Xe gas-transfer spectroscopy in patients with idiopathic pulmonary fibrosis. *J Appl Physiol* 2014;117:577–85.
18 Stewart NJ, Leung G, Norquay G, *et al*. Experimental validation of the hyperpolarized 129Xe chemical shift saturation recovery technique in healthy volunteers and subjects with interstitial lung disease. *Magn Reson Med* 2014;74:196–207.
19 Patz S, Muradian I, Hrovat MI, *et al*. Human pulmonary imaging and spectroscopy with hyperpolarized 129Xe at 0.2T. *Acad Radiol* 2008;15:713–27.
20 Ruppert K, Brookeman JR, Hagspiel KD, *et al*. Probing lung physiology with xenon polarization transfer contrast (XTC). *Magn Reson Med* 2000;44:349–57.
21 Månsson S, Wolber J, Driehuys B, *et al*. Characterization of diffusing capacity and perfusion of the rat lung in a lipopolysaccaride disease model using hyperpolarized 129Xe. *Magn Reson Med* 2003;50:1170–9.
22 Qing K, Ruppert K, Jiang Y, *et al*. Regional mapping of gas uptake by blood and tissue in the human lung using hyperpolarized xenon-129 MRI. *J Magn Reson Imaging* 2014;39:346–59.
23 Kaushik SS, Robertson SH, Freeman MS, *et al*. Single-breath clinical imaging of hyperpolarized 129Xe in the airspaces, barrier, and red blood cells using an interleaved 3D radial 1-point dixon acquisition. *Magn Reson Med* 2016;75:1434–43.
24 Wang Z, Robertson SH, Wang J, *et al*. Quantitative analysis of hyperpolarized (129) Xe gas transfer MRI. *Med Phys* 2017;44:2415–28.
25 Ley B, Elicker BM, Hartman TE, *et al*. Idiopathic pulmonary fibrosis: CT and risk of death. *Radiology* 2014;273:570–9.
26 Hunninghake GW, Lynch DA, Galvin JR, *et al*. Radiologic findings are strongly associated with a pathologic diagnosis of usual interstitial pneumonia. *Chest* 2003;124:1215–23.
27 Nishimura K, Kitaichi M, Izumi T, *et al*. Usual interstitial pneumonia: histologic correlation with high-resolution CT. *Radiology* 1992;182:337–42.
28 He M, Robertson SH, Kaushik SS, *et al*. Dose and pulse sequence considerations for hyperpolarized (129)Xe ventilation MRI. *Magn Reson Imaging* 2015;33:877–85.
29 Kaushik SS, Robertson SH, Freeman MS, *et al*. Single-breath clinical imaging of hyperpolarized (129)Xe in the airspaces, barrier, and red blood cells using an interleaved 3D radial 1-point dixon acquisition. *Magn Reson Med* 2016;75:1434–43.
30 Kaushik SS, Freeman MS, Cleveland ZI, *et al*. Probing the regional distribution of pulmonary gas exchange through single-breath gas- and dissolved-phase 129Xe MR imaging. *J Appl Physiol* 2013;115:850–60.
31 He M, Driehuys B, Que LG, *et al*. Using hyperpolarized 129Xe MRI to quantify the pulmonary ventilation distribution. *Acad Radiol* 2016;23:1521–31.
32 Qing K, Mugler JP, Altes TA, *et al*. Assessment of lung function in asthma and COPD using hyperpolarized 129Xe chemical shift saturation recovery spectroscopy and dissolved-phase MRI. *NMR Biomed* 2014;27:1490–501.
33 Jacob J, Bartholmai BJ, Rajagopalan S, *et al*. Mortality prediction in idiopathic pulmonary fibrosis: evaluation of computer-based CT analysis with conventional severity measures. *Eur Respir J* 2017;49:1601011.
34 Ash SY, Harmouche R, Vallejo DL, *et al*. Densitometric and local histogram based analysis of computed tomography images in patients with idiopathic pulmonary fibrosis. *Respir Res* 2017;18:45.
35 Cleveland ZI, Virgincar RS, Qi Y, *et al*. 3D MRI of impaired hyperpolarized 129Xe uptake in a rat model of pulmonary fibrosis. *NMR Biomed* 2014;27:1502–14.
36 West JB, Dollery CT, Naimark A. Distribution of blood flow in isolated lung; relation to vascular and alveolar pressures. *J Appl Physiol* 1964;19:713–24.
37 Hsia CC, Hyde DM, Weibel ER. Lung structure and the intrinsic challenges of gas exchange. *Compr Physiol* 2016;6:827–95.
38 Katzenstein AL, Myers JL. Idiopathic pulmonary fibrosis: clinical relevance of pathologic classification. *Am J Respir Crit Care Med* 1998;157(4 Pt 1):1301–15.
39 Smith M, Dalurzo M, Panse P, *et al*. Usual interstitial pneumonia-pattern fibrosis in surgical lung biopsies. Clinical, radiological and histopathological clues to aetiology. *J Clin Pathol* 2013;66:896–903.
40 Ochs M, Nyengaard JR, Jung A, *et al*. The number of alveoli in the human lung. *Am J Respir Crit Care Med* 2004;169:120–4.
41 Stam H, Hrachovina V, Stijnen T, *et al*. Diffusing capacity dependent on lung volume and age in normal subjects. *J Appl Physiol* 1994;76:2356–63.
42 Janssens JP, Pache JC, Nicod LP. Physiological changes in respiratory function associated with ageing. *Eur Respir J* 1999;13:197–205.